

Nuclear size, electric monopole transitions, and the location of 0_2^+ states

B. Maheshwari,^{1,*} K. Nomura,^{2,3} and P. Van Isacker¹

¹*Grand Accélérateur National d'Ions Lourds, CEA/DSM-CNRS/IN2P3,
Bvd Henri Becquerel, BP 55027, F-14076 Caen, France*

²*Department of Physics, Hokkaido University, Sapporo 060-0810, Japan*

³*Nuclear Reaction Data Center, Hokkaido University, Sapporo 060-0810, Japan*

(Dated: February 10, 2025)

The work addresses the isotopic shift of nuclear radii for the even-even $^{36-52}\text{Ca}$ isotopes using the interacting boson model (IBM) that includes the mixing from normal and intruder configurations. We obtain a good agreement between the calculated and experimental data, particularly for the dip at ^{48}Ca . A direct correlation between nuclear size and electric monopole transitions is established to compute the electric monopole transition strengths, $\rho^2(E0)$. We further study the isotopic shift for the even-even $^{32-46}\text{Ar}$ and $^{44-50}\text{Ti}$ isotopes.

I. INTRODUCTION

An important global property of an atomic nucleus is its size, that is, its (charge) radius, which carries knowledge about the nucleonic dynamics inside the nucleus due to the nuclear force. Similar to electrons in an atom, nucleons in a nucleus occupy discrete quantum levels with shell gaps at nucleon numbers 2, 8, 20, 28, 50, 82, and 126 (colloquially known as “magic” numbers). At these nucleon numbers a nucleus experiences an increased stability as compared to neighboring nuclei, which can influence its charge radius. The spin-orbit interaction plays a crucial role in the stability of nuclei since it favors single-particle levels, denoted as j_+ , with an orbital angular momentum l that is aligned with the intrinsic spin s of the nucleon. For heavier nuclei, with mass numbers $A \gtrsim 50$, the effect of the spin-orbit interaction can be so strong that a j_+ orbital with high l intrudes into a lower-lying shell of the harmonic oscillator. This mechanism explains the magic numbers 28 and higher that are observed in nuclei close to the stability line [1]. Nevertheless, a fundamental understanding of the evolution of shell gaps in neutron-rich or neutron-deficient nuclei, far removed from the stability line, is still lacking [2–6]. In particular, their impact on charge radii remains a challenge for modern experimental and theoretical nuclear physics.

Due to recent advances in radioactive-ion-beam production, the charge radii of the calcium isotopes ($Z = 20$) are now known over a long range, from proton-rich ^{36}Ca [7] to neutron-rich ^{52}Ca [8]. The measurements support the doubly-magic nature of ^{40}Ca and ^{48}Ca , which have almost equal charge radii [8]. The local maximum of the charge radius of ^{44}Ca and its very steep increase beyond ^{48}Ca pose a serious challenge for nuclear theory. If the ground states of even-even nuclei can be described in terms of nucleonic pairs, as is the basic assumption of the interacting boson model (IBM) [9], it is tempting to model the evolution of charge radii with bosons [10–13].

Weak shell gaps favor the formation of deformed shapes [14–17] as well as the occurrence of shape coexistence [18–21]. In the long chain of even-even $^{36-52}\text{Ca}$ isotopes, only one isotope, namely doubly-magic ^{40}Ca , has a first-excited state with angular momentum $J^\pi = 0^+$, which is a signature of shape coexistence. This 0_2^+ isomeric state has a half-life of 2.17 ns [22, 23] and is interpreted as a four-particle-four-hole excitation [24]. The 0_2^+ state in another doubly-magic Ca isotope, ^{48}Ca , exists with a relatively shorter half-life of 0.22 ns [24] with a 22.5% of $E0$ branch. The 0_2^+ state in ^{42}Ca is also known with a shorter half-life of 0.38 ns [24] but with a weak $E0$ branch. Electric monopole ($E0$) transitions from 0_2^+ to the ground state are known in the $^{40,42,44,48}\text{Ca}$ isotopes [25] and their complementary $\rho^2(E0)$ values follow an inverted parabola with minima for $^{40,48}\text{Ca}$. Although in most Ca isotopes an $E2$ transition is possible to a lower-lying 2^+ state, the $E0$ behavior is possibly correlated with the 0_2^+ half-lives especially when $B(E2; 0_2^+ \rightarrow 2_1^+)$ is in the order of ≤ 10 W.u., hinting at the importance of the $E0$ transition to determine whether the 0_2^+ state is isomeric or not. $E0$ transitions connecting two 0^+ states are special since no photon emission is allowed and the decay necessarily proceeds via electron conversion and/or electron-positron pair emission [21].

In this article we aim to correlate the location of the 0_2^+ state with the size of the nucleus (i.e., its charge radius) using a version of the IBM that incorporates the mechanism of coexistence and configuration mixing, referred hereafter as IBM-CM [26]. The puzzling behavior of the charge radii of the even-even $^{36-52}\text{Ca}$ isotopes so far has not been considered in the context of IBM, to the best of our knowledge. Electric-monopole transition strengths are also calculated in the same framework and the double magicity of $^{40,48}\text{Ca}$ is also explored [4, 6]. We further present similar results for the even-even $^{32-48}\text{Ar}$ and $^{44-50}\text{Ti}$ isotopes having two sd proton holes and two pf proton particles with respect to Ca isotopes, respectively.

* bhoomika.physics@gmail.com

II. FORMALISM

The interacting boson model (IBM) [27] is comprised of s and d bosons with angular momenta 0^+ and 2^+ , representing monopole and quadrupole pairs of valence nucleons, respectively [9, 28]. The total number of bosons, denoted as $n_b = n_s + n_d$, is determined by the microscopic interpretation of active valence nucleons, $n_b = n_\pi + n_\nu$ where n_π (n_ν) equals the number of proton (neutron) particle or hole pairs counted from the nearest closed shell. A distinctive feature of the IBM is its ability to furnish the U(6) algebra with generators formed by s and d_μ ($\mu = 0, \pm 1, \pm 2$) bosons. The U(6) algebra is subsequently reduced to the U(5), SU(3), and SO(6) subalgebras, providing vibrational, rotational and γ -unstable spectra, respectively. The IBM Hamiltonian employed for phenomenological description of low-energy states is expressed as follows:

$$\hat{H} = \epsilon \hat{n}_d + a_1 \hat{L} \cdot \hat{L} + a_2 \hat{Q} \cdot \hat{Q}, \quad (1)$$

where ϵ stands for the energy of a single d boson relative to that of an s boson and $\hat{n}_d = d^\dagger \cdot d$ denotes the d -boson number operator, with $\tilde{d}_\mu = (-1)^\mu d_{-\mu}$. The second term with strength a_1 represents the SO(3) Casimir operator, with $\hat{L} = \sqrt{10}[d^\dagger \times \tilde{d}]^{(1)}$. The third term with strength a_2 is the quadrupole-quadrupole interaction inducing quadrupolar deformation. The corresponding operator reads $\hat{Q} = s^\dagger \tilde{d} + d^\dagger \tilde{s} + \chi[d^\dagger \times \tilde{d}]^{(2)}$, where χ is a parameter which determines whether the nuclear shape is prolate ($\chi < 0$) or oblate ($\chi > 0$) [9].

In the IBM-CM several independent Hamiltonians are introduced for systems with $n_b, n_b + 2, n_b + 4, \dots$ bosons, associated with 0p-0h, 2p-2h, 4p-4h, \dots particle-hole excitations, respectively. The unperturbed eigenstates of the separate Hamiltonians are allowed to mix in order to incorporate configuration mixing [26]. Here we consider two configurations, i.e., the normal or regular $[n_b]$ and the intruder $[n_b + 2]$ configuration. The full IBM-CM Hamiltonian reads

$$\hat{H}' = \hat{H}_{\text{reg}} + (\hat{H}_{\text{int}} + \Delta) + \hat{V}_{\text{mix}}, \quad (2)$$

where \hat{H}_{reg} and \hat{H}_{int} represent the Hamiltonians for the regular (0p-0h) and intruder (2p-2h) boson spaces, respectively, and each has the form given by Eq. (1). Δ represents the energy needed to promote a nucleon pair from a major oscillator shell to the next. The last term in Eq. (2) is the interaction which admixes the different boson spaces and which is given by

$$\hat{V}_{\text{mix}} = \alpha (s^\dagger s^\dagger + \tilde{s} \tilde{s}) + \beta [d^\dagger \times d^\dagger + \tilde{d} \times \tilde{d}]^{(0)}, \quad (3)$$

where α and β parametrize the mixing strength. In all calculations presented here fixed values for α and β are taken for each isotopic chain, which in addition are assumed to be equal, $\alpha = \beta$. ^{48}Ca is an exception to this assumption. The Hamiltonian (2) is diagonalized in the full $[n_b] \oplus [n_b + 2]$ space to obtain excitation energies and

wave functions [29]. A common core of ^{40}Ca is used for the IBM-CM calculations.

The question arises whether a version of the IBM should be used that respects isospin invariance. Specifically, in IBM-3 [30] a neutron-proton boson with isospin $T=1$ is introduced besides the usual neutron-neutron and proton-proton bosons of IBM-2, and in IBM-4 [31] one considers additionally a neutron-proton boson with $T=0$. Such more elaborate versions of the IBM are important in nuclei with valence neutrons and protons in the same orbitals since it allows the definition of the isospin quantum number for a boson system. As a result, these extended boson models have a more solid microscopic connection with the shell model. However, so far no version of IBM-3 or IBM-4 has been developed that incorporates both regular and intruder configurations. Also, a procedure is known to project from IBM-3 to IBM-1 [32], and in the latter system the mixing of several configurations is well established.

The procedure of fitting the IBM-CM Hamiltonian parameters is described in Ref. [19] and all parameters used for the present analysis are listed in Table I. The calculated level energies are compared with the experimental data, wherever available, in Table II. An overall agreement between the experimental data and calculated results has been achieved by fixing ϵ based on the location of the 2_1^+ state, and Δ based on that of the 0_2^+ state. The energies of other levels in the spectra are then determined from the a_1 and a_2 parameters. The spectra of most of the fitted nuclei are compatible with $\chi = 0$ in both the $[n_b]$ and $[n_b + 2]$ spaces with the exception of the $^{44,50}\text{Ca}$, $^{32,34,36}\text{Ar}$, and $^{44,46,48}\text{Ti}$ isotopes. The results for the $^{42,44,46}\text{Ca}$ isotopes have already been discussed in Ref. [19]. In ^{50}Ca , a prolate deformed SU(3) $[n_b + 2]$ space (with $\chi = -1.33$) is assumed. In $^{32,34}\text{Ar}$ an oblate deformed SU(3) $[n_b]$ space (with $\chi = +1.33$) together with a prolate deformed SU(3) $[n_b + 2]$ space (with $\chi = -1.33$) is assumed. In ^{36}Ar an oblate deformed SU(3) $[n_b]$ space (with $\chi = +1.33$) is assumed with a vibrational U(5) $[n_b + 2]$ space. In the stable ^{38}Ar isotope and onwards $\chi = 0$ is found to be sufficient in both $[n_b]$ and $[n_b + 2]$ spaces. This is also consistent with the shape description of these lighter Ar isotopes in the literature, see the recent review [21]. In $^{44,46,48}\text{Ti}$ a $[n_b]$ space is assumed with $\chi = -1$. It may be noted that the fitting of parameters is primarily based on the energies of few lower-lying levels. Such parameters may likely to fall insufficient to describe the other observables such as $B(E2)$ s.

In the IBM the charge radius operator is taken as [9–11]

$$\hat{T}(r^2) = \langle r^2 \rangle_c + \kappa_{\text{reg}} \hat{n}_b + \eta_{\text{reg}} \frac{\hat{n}_d}{\hat{n}_b}, \quad (4)$$

where the first term is the square of the charge radius of the core nucleus. The second term refers to the increase of the charge radius due to the addition of two nucleons. The third term describes the contribution arising from

the deformation. The same expression is valid for the intruder $[n_b + 2]$ configuration with the parameters κ_{int} and η_{int} for the second and third terms, respectively. In the standard IBM the increase of the charge radius due to the addition of two nucleons is assumed to be linear as it is taken proportional to the number of bosons. Note, however, that in order to ensure this linear behavior at the middle of the valence shell a change of sign of the parameter κ_{reg} is needed since the interpretation of the bosons changes from a pair of particles to a pair of holes [9]. In IBM-CM, this linear behavior breaks down especially when one shifts from $[n_b]$ space to the $[n_b + 2]$ space. To maintain in the IBM-CM a linear increase of the second term in Eq. (4) with the number of valence nucleon pairs, it is necessary to impose the relation $\kappa_{\text{int}} = \frac{n_b}{n_b + 2} \kappa_{\text{reg}}$ [33]. One calculates, therefore, the isotopic shift of the charge radius with respect to the core as follows:

$$\begin{aligned} \delta \langle r^2 \rangle^A &= \langle \hat{T}(r^2) \rangle_{0_1^+}^A - \langle r^2 \rangle_c \\ &= 2\kappa_{\text{reg}} n_b + \frac{\eta_{\text{reg}}}{n_b} \langle 0_1^+ | \hat{n}_d | 0_1^+ \rangle_{n_b}^A \\ &\quad + \frac{\eta_{\text{int}}}{n_b + 2} \langle 0_1^+ | \hat{n}_d | 0_1^+ \rangle_{n_b + 2}^A. \end{aligned} \quad (5)$$

In this framework $E0$ transitions can be directly correlated with the nuclear size, that is, with the charge radius of the ground state. The electric monopole transition strength $\rho(E0)$ between the second-excited 0_2^+ and ground 0_1^+ states in the $[n_b] \oplus [n_b + 2]$ space is given by

$$\begin{aligned} \rho(E0; 0_2^+ \rightarrow 0_1^+) &= \frac{2en_b}{eR^2} \left(\frac{\eta_{\text{reg}}}{n_b} \langle 0_1^+ | \hat{n}_d | 0_2^+ \rangle_{n_b}^A \right. \\ &\quad \left. + \frac{\eta_{\text{int}}}{n_b + 2} \langle 0_1^+ | \hat{n}_d | 0_2^+ \rangle_{n_b + 2}^A \right), \end{aligned} \quad (6)$$

where $R = 1.02A^{1/3}$ fm is the radius of an ideal-spherical nucleus and the coefficient 1.02 is chosen for the lighter-mass nuclei based on the charge radius of ^{40}Ca [34]. The number of active valence nucleons appears as $2n_b$ in the numerator of Eq. (6). The first and second terms arise due to the contributions from the deformation in the respective $[n_b]$ and $[n_b + 2]$ spaces. The $E0$ strengths are usually expressed in terms of the square of Eq. (6), $\rho^2(E0)$, which is a dimensionless quantity. The same parameters η_{reg} and η_{int} , as obtained from the isotopic shifts by the application of Eq. (5), are used to calculate $E0$ strengths, implying therefore a direct correlation between charge radii and electric monopole transitions.

To complement the discussion on the location of 0_2^+ state, also results of the NSM are presented. All calculations are performed with the KSHELL code [35]. The center-of-mass correction is taken care of as default. The results for $^{36,38}\text{Ca}$ are obtained with the SDPF-MU interaction [36] with a full sd ($sdpf$) valence space for the protons (neutrons). The NSM calculations for the even-even $^{42-52}\text{Ca}$ isotopes are performed in the pf valence space with the KB3G interaction [37]. The NSM calculations

for $^{32-36}\text{Ar}$ are performed with the SDPF-MU interaction in the sd ($sdpf$) valence space for protons (neutrons) while the sd (pf) valence space is used for protons (neutrons) in $^{40-46}\text{Ar}$. This valence space is usually found to be sufficient for these Ar isotopes, especially for the yrast spectra [38]. In $^{44-50}\text{Ti}$ the NSM calculations are performed with the KB3G interaction in the pf valence space for both protons and neutrons.

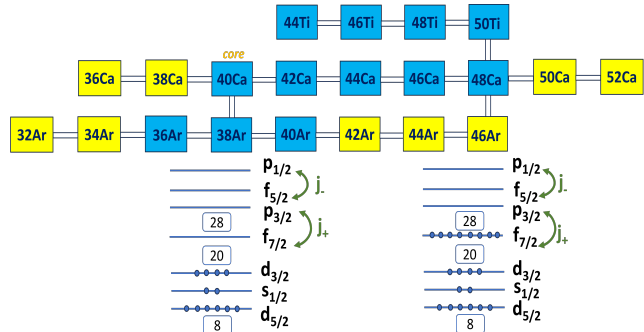


FIG. 1. (Color online) Schematic picture of the region of interest which includes nuclei with a known charge radius [7, 8, 39–41]. Stable isotopes with natural abundances are in blue and others are in yellow [42, 43]. Active single-particle orbitals are also shown together with the shell gaps. This includes $N = 28$, the first magic gap due to the spin-orbit interaction. The two level schemes are just to show the Z , or $N = 20$ and 28 closed shell configurations. The vertical double lines connecting nuclei is depicted for closed shells, while the horizontal ones simply refer to a given isotopic chain.

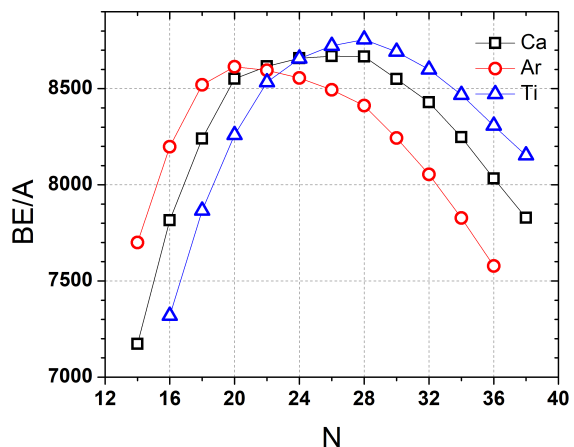


FIG. 2. (Color online) Empirical binding energy per nucleon (BE/A) for even-even Ca, Ar, and Ti isotopes [42].

TABLE I. Parameters of the IBM-CM Hamiltonian for the nuclei considered in this study.

Nucleus	ϵ (MeV)		a_1 (MeV)		a_2 (MeV)		χ		$\alpha = \beta$ (MeV)	Δ (MeV)
	$[n_b]$	$[n_b + 2]$	$[n_b]$	$[n_b + 2]$	$[n_b]$	$[n_b + 2]$	$[n_b]$	$[n_b + 2]$		
^{36}Ca	1.1	1.3	0.32	0.10	-0.05	-0.05	0.0	0.0	0.25	1.5
^{38}Ca	0.9	0.7	0.18	0.02	-0.05	-0.03	0.0	0.0	0.25	1.5
^{42}Ca	0.4	0.4	0.20	-0.01	-0.05	-0.05	0.0	0.0	0.25	1.0
^{44}Ca	0.6	0.4	0.05	-0.004	-0.05	-0.05	0.0	-1.0	0.25	1.1
^{46}Ca	0.8	0.8	0.18	-0.04	-0.05	-0.05	0.0	0.0	0.25	1.0
^{48}Ca	2.1	2.2	0.60	-0.14	-0.035	-0.06	0.0	0.0	0.30	2.0
^{50}Ca	0.8	1.95	0.09	0.10	-0.05	-0.15	0.0	-1.33	0.25	0.65
^{32}Ar	1.35	0.95	0.18	0.05	-0.125	-0.08	1.33	-1.33	0.15	1.55
^{34}Ar	1.35	0.95	0.18	0.05	-0.125	-0.08	1.33	-1.33	0.15	1.55
^{36}Ar	1.25	1.15	0.15	-0.06	-0.138	-0.065	1.33	0.0	0.15	1.55
^{38}Ar	1.35	0.9	0.18	0.015	0.045	0.025	0.0	0.0	0.15	1.55
^{40}Ar	1.35	0.35	0.033	0.001	0.065	0.0	0.0	0.0	0.15	1.55
^{42}Ar	0.95	0.9	0.025	0.005	0.038	0.025	0.0	0.0	0.15	1.55
^{44}Ar	0.95	0.9	0.015	0.005	0.04	0.025	0.0	0.0	0.15	1.55
^{46}Ar	1.15	0.9	0.075	0.005	0.0	0.005	0.0	0.0	0.15	1.55
^{44}Ti	0.7	0.5	0.018	0.014	-0.05	-0.05	-1.0	0.0	0.30	0.90
^{46}Ti	0.6	0.5	0.02	-0.02	-0.12	-0.095	-1.0	0.0	0.30	0.90
^{48}Ti	0.6	0.5	0.013	-0.018	-0.18	-0.16	-1.0	0.0	0.30	0.90
^{50}Ti	1.65	1.45	-0.06	0.08	0.01	0.06	0.0	0.0	0.30	0.90

TABLE II. Experimental energies [42] and energies calculated in the IBM-CM of some yrast and yrare levels in the nuclei considered in this study.

Nucleus	Experimental E(MeV)						Calculated E(MeV)					
	0_1^+	0_2^+	2_1^+	2_2^+	4_1^+	4_2^+	0_1^+	0_2^+	2_1^+	2_2^+	4_1^+	4_2^+
^{36}Ca	0.0	2.830	3.045	4.710			0.0	2.853	3.163	4.737	8.102	9.424
^{38}Ca	0.0	3.083	2.213	3.683	5.816*		0.0	3.074	2.202	3.863	4.883	5.823
^{40}Ca	0.0	3.352	3.904	5.248	5.278	6.507			—core—			
^{42}Ca	0.0	1.837	1.524	2.424	2.752	3.253	0.0	1.951	1.637	2.463	2.596	3.396
^{44}Ca	0.0	1.883	1.157	2.656	2.283	3.044	0.0	1.808	1.041	2.053	2.309	3.204
^{46}Ca	0.0	2.423	1.346	3.022	2.574	3.859	0.0	2.304	1.577	2.777	2.644	3.810
^{48}Ca	0.0	4.283	3.831	6.105*	4.503		0.0	4.320	3.792	6.184	4.638	7.075
^{50}Ca	0.0	4.475*	1.026	3.002*	4.515*		0.0	4.301	1.225	6.143	3.996	9.399
^{32}Ar	0.0		1.867				0.0	2.525	1.914	3.008	4.372	5.990
^{34}Ar	0.0	3.873	2.091	3.287	4.631 [†]		0.0	2.595	2.160	3.253	4.668	6.469
^{36}Ar	0.0		1.970	4.440	4.414	6.136	0.0	2.958	2.192	4.022	4.439	6.057
^{38}Ar	0.0	3.376	2.167	3.936	5.349	6.053*	0.0	3.312	2.260	4.294	5.298	5.998
^{40}Ar	0.0	2.120	1.460	2.524	2.892	3.515	0.0	2.239	1.451	2.427	2.831	3.404
^{42}Ar	0.0		1.208	2.485	2.413*	3.096	0.0	1.908	1.165	2.024	2.370	3.040
^{44}Ar	0.0	0.750?	1.158	1.610*	2.746*		0.0	2.109	1.194	2.148	2.354	3.141
^{46}Ar	0.0		1.570	3.489	3.892		0.0	2.400	1.629	2.834	3.793	5.004
^{44}Ti	0.0	1.904	1.083	2.530	2.454	3.364	0.0	2.024	1.041	2.203	2.400	3.562
^{46}Ti	0.0	2.611	0.889	2.961	2.009	3.848*	0.0	2.525	0.886	2.251	2.108	3.570
^{48}Ti	0.0	2.997	0.983	2.421	2.295	3.239	0.0	3.092	0.889	2.410	2.186	3.963
^{50}Ti	0.0	3.868	1.553	4.309	2.674	5.186	0.0	3.692	1.659	3.466	2.716	4.412

* : Spin-parity assignment is not confirmed.

? : Based on NNDC evaluators [42].

[†] : A. R. L. Kennington *et al.* [44]

III. DISCUSSION

Figure 1 refers to the region of interest in and around the $Z = 20$ shell closure, from even-even Ca ($Z = 20$) to Ar ($Z = 18$) and Ti ($Z = 22$) isotopes, for which data on charge radii are available [7, 8, 39–41]. Both ^{40}Ca ($Z = 20, N = 20$) and ^{48}Ca ($Z = 20, N = 28$) are (almost) stable, consistent with their doubly-magic

character, while in the Ar and Ti isotopes the semi-magic ^{38}Ar ($Z = 18, N = 20$) and ^{50}Ti ($Z = 22, N = 28$) are stable but ^{46}Ar ($Z = 18, N = 28$) and ^{42}Ti ($Z = 22, N = 20$) are not.

Figure 2 shows the empirical binding energy per nucleon (BE/A) for even-even Ca, Ar, and Ti isotopes [42]. The binding energy per nucleon is rather flat for the Ca isotopes between doubly-magic ^{40}Ca and ^{48}Ca , and it

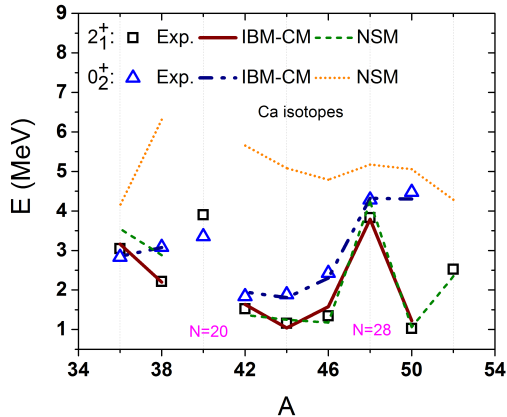


FIG. 3. (Color online) Experimental [24] and calculated energies E of the yrast 2_1^+ and yrare 0_2^+ levels in the even-even $^{36-52}\text{Ca}$ isotopes.

steeply drops off outside this region. In contrast, in the Ar and Ti isotopes, the semi-magic ^{38}Ar and ^{50}Ti have maximal binding energy per nucleon while ^{46}Ar and ^{42}Ti , although conceivably also semi-magic with $N = 28$ and $N = 20$, respectively, have a much lower BE/A . The question thus arises whether this characteristic behavior of BE/A is reflected in the evolution of the charge radii.

A. The calcium isotopes

We first apply the IBM-CM to the even-even $^{36-52}\text{Ca}$ isotopes with parameters as listed in Table I. The doubly-magic nucleus ^{40}Ca is assumed to be the inert core and hence the boson numbers for the regular configuration in the even-even $^{42-52}\text{Ca}$ isotopes are 1, 2, 3, ..., 6, respectively. An overall good agreement between the experimental and calculated low-energy levels is achieved, as listed in Table II. The predicted and experimental energies of the 2_1^+ and 0_2^+ levels are compared in Fig. 3. The present calculation, which includes mixing of regular and intruder configurations, agrees nicely with the experimental energies of the 2_1^+ and 0_2^+ levels in the Ca isotopes. In ^{52}Ca , the experimental data are quite limited to fix the IBM-CM analysis which is therefore not performed. Also, the measured level energy of 2_1^+ in ^{50}Ca displays a sharp dip at 1.026 MeV, to be compared with the surrounding isotopes, namely the doubly-magic ^{48}Ca (2_1^+ at 3.831 MeV) and ^{52}Ca (2_1^+ at 2.563 MeV). This suggests to measure low-energy levels in ^{52}Ca , especially since this nuclide is getting attention as regards a potential $N = 32$ sub-shell closure [5, 8].

In a recent experimental work on the structure of ^{36}Ca [45] the importance of core excitations was pointed out, especially for the second-excited 0_2^+ state. The present IBM-CM analysis supports this analysis. Notably, the 0_2^+ levels in $^{36,38}\text{Ca}$ are at almost equal energies

(see Table II) whereas the 2_1^+ level in ^{36}Ca is at higher energy than in ^{38}Ca . The latter may be related to a possible $N = 16$ shell closure [5]. In ^{38}Ca the yrast 2_1^+ state is most likely dominated by the $d_{3/2}^2$ configuration, similar to ^{50}Ca where it is dominated by $p_{3/2}^2$, both involving $j = 3/2$. Similarly, the 0_2^+ levels in $^{36,38}\text{Ca}$ are at similar energies while the 2_1^+ excitation energies are vastly different. The 2_1^+ energy is indicative of shell gaps whereas that of 0_2^+ is sensitive to possible core excitations. Shell gaps, when identified with effective single-particle energies, are known to evolve with nucleon number but they may also state-dependent in a single nuclide due to a self-organization mechanism [47]. The structure of the 2_1^+ and 0_2^+ states is therefore crucial for understanding the evolution of shell gaps in nuclei.

It may be recalled that the NSM interactions usually explain the variation of the excitation energy of the 2_1^+ level but overestimates the location of 0_2^+ states in pf-shell nuclei, such as the case in the $^{42,44,46}\text{Ca}$ isotopes [19], indicating the importance of core excitations for the yrare states in Ca. The present set of NSM calculations in Fig. 3 is reliable for yrast states only.

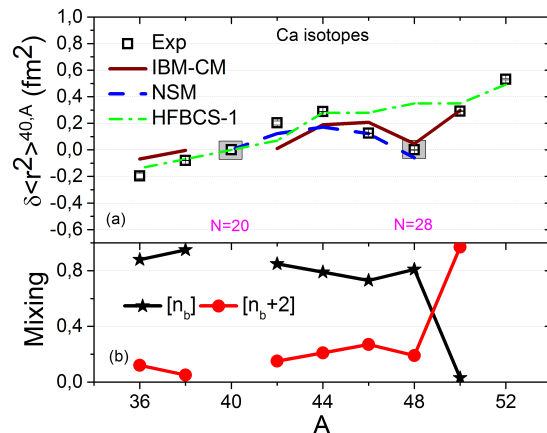


FIG. 4. (Color online) (a) Experimental [7, 8] and calculated isotopic shifts in the even-even $^{36-52}\text{Ca}$ isotopes. Results of IBM-CM, NSM [46], and HFBCS-1 [51] calculations are shown. The stable isotopes and the doubly-magic $^{40,48}\text{Ca}$ are shown in grey. The error bars on data are within the size of symbol. (b) The mixing of the $[n_b]$ and $[n_b + 2]$ spaces for the ground states of the even-even $^{36-52}\text{Ca}$ isotopes.

With wave functions fixed from level energies, one can compute the charge radii using Eq. (4), and the corresponding isotopic shift (of the charge radii) using Eq. (5). The parameter $\kappa_{\text{reg}} = 0.0005 \text{ fm}^2$ is adjusted to the overall slope of the isotopic shift for the even-even $^{42-52}\text{Ca}$ isotopes but otherwise the main features are controlled by two parameters, $\eta_{\text{reg}} = 8.69 \text{ fm}^2$ and $\eta_{\text{int}} = 0.59 \text{ fm}^2$. The absolute values of these parameters are then used to compute the isotopic shifts of $^{36,38}\text{Ca}$ but taken to be negative since in these isotopes bosons correspond to hole pairs. The corresponding IBM-CM isotopic shifts

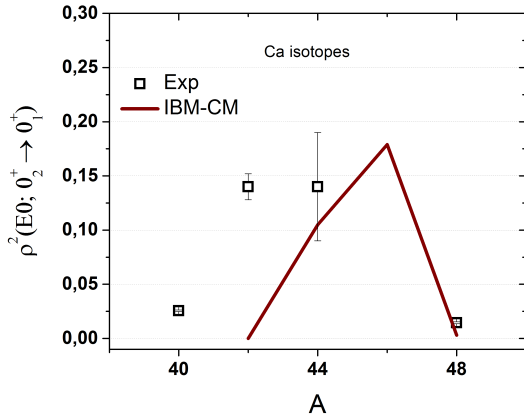


FIG. 5. (Color online) Experimental [25] and calculated $\rho^2(E0; 0_2^+ \rightarrow 0_1^+)$ values within the IBM-CM in the even-even ${}^{36-52}\text{Ca}$ isotopes.

are compared with the data in the even-even ${}^{36-52}\text{Ca}$ isotopes in Fig. 4(a). The calculated results are in an overall agreement with the data for the long chain of Ca isotopes. The IBM-CM does not explain the isotopic shift of ${}^{38,42}\text{Ca}$ due to limited number of active bosons, which influences the contributions of \hat{n}_d matrix elements. However, the dip for ${}^{48}\text{Ca}$ and the sharp increase at ${}^{50}\text{Ca}$ is well reproduced due to the change in the dominant wave function, as depicted in Fig. 4(b).

TABLE III. The mixing probabilities of the $[n_b]$ and $[n_b + 2]$ spaces calculated in IBM-CM for the 2_1^+ and 0_2^+ states.

Nucleus	2_1^+		0_2^+	
	$[n_b]$	$[n_b + 2]$	$[n_b]$	$[n_b + 2]$
${}^{36}\text{Ca}$	0.83	0.17	0.14	0.86
${}^{38}\text{Ca}$	0.93	0.07	0.05	0.95
${}^{40}\text{Ca}$	—core—			
${}^{42}\text{Ca}$	0.52	0.48	0.15	0.85
${}^{44}\text{Ca}$	0.70	0.30	0.75	0.25
${}^{46}\text{Ca}$	0.45	0.55	0.81	0.19
${}^{48}\text{Ca}$	0.22	0.78	0.25	0.75
${}^{50}\text{Ca}$	0.02	0.98	0.10	0.90
${}^{32}\text{Ar}$	0.86	0.14	0.14	0.86
${}^{34}\text{Ar}$	0.85	0.15	0.15	0.85
${}^{36}\text{Ar}$	0.95	0.05	0.97	0.03
${}^{38}\text{Ar}$	0.99	0.01	0.01	0.99
${}^{40}\text{Ar}$	0.93	0.07	0.91	0.09
${}^{42}\text{Ar}$	0.97	0.03	0.98	0.02
${}^{44}\text{Ar}$	0.96	0.04	0.97	0.03
${}^{46}\text{Ar}$	0.92	0.08	0.95	0.05
${}^{44}\text{Ti}$	0.72	0.28	0.81	0.19
${}^{46}\text{Ti}$	0.56	0.44	0.75	0.25
${}^{48}\text{Ti}$	0.34	0.66	0.64	0.36
${}^{50}\text{Ti}$	0.91	0.09	0.85	0.15

There is a blocking effect for the core excitations as one reaches ${}^{48}\text{Ca}$. It may be related to the blocking of excitations from the d to f orbital as neutrons are fully filling the $f_{7/2}$ at $N = 28$ [48]. This also contributes to

the stability of ${}^{48}\text{Ca}$, and to a smaller nuclear size. The states in nuclei in the middle of $f_{7/2}$, ${}^{44,46}\text{Ca}$, become more collective from the mixing between the regular and intruder spaces of the IBM-CM, as shown in Fig. 4(b). This involves a change in the neutron-neutron interaction in going from ${}^{42}\text{Ca}$, involving mainly the $d_{3/2}$ and $f_{7/2}$ orbitals, to ${}^{48}\text{Ca}$, involving mainly the $f_{7/2}$ and $p_{3/2}$ orbitals. Below ${}^{48}\text{Ca}$, the coupling between the d - f orbitals, which share the same principal quantum number, results in a more attractive force, causing a contraction of the charge radius [4]. In contrast, above ${}^{48}\text{Ca}$ the coupling between the f - p orbitals, which have different principal quantum numbers, leads to a larger charge radius. This is why the kink in the charge radii around ${}^{40}\text{Ca}$ is softer than the one around ${}^{48}\text{Ca}$, which is therefore explained by the fact that $N = 28$ is the first magic gap due to the spin-orbit interaction. This also explains why the 0_2^+ state has a longer half-life in ${}^{40}\text{Ca}$ than it has in ${}^{48}\text{Ca}$. Figure 4(b) presents the mixing of the $[n_b]$ and $[n_b + 2]$ spaces in the IBM-CM for the ground states of the even-even ${}^{36-52}\text{Ca}$ isotopes. In ${}^{50,52}\text{Ca}$ the major component of the ground state is in the $[n_b + 2]$ space which leads to a larger nuclear size, as is observed. For completeness the $[n_b]$ and $[n_b + 2]$ probabilities for the 2_1^+ and 0_2^+ states are listed in Table III. The mixing of two spaces is clearly visible but it is not always the case that the 0_2^+ state is dominated by $[n_b + 2]$ space.

We also show in Fig. 4 the NSM results adopted from Caurier *et al.* [46] for the isotopic shifts of the even-even ${}^{40-48}\text{Ca}$ isotopes. Such NSM estimates explain the dip in charge radii at ${}^{48}\text{Ca}$ using the number of protons lifted from sd - to the pf - shell. A similar exercise with available $sdpf$ interactions using the prescription of ref. [46] is not suitable, since these effective interactions were mainly designed for neutron-rich sd -shell nuclei and can not reproduce the location of 0_2^+ state, as depicted for ${}^{36,38}\text{Ca}$ isotopes in Fig. 3. This already hints at a possible connection between the charge radius and the location of 0_2^+ state, since the interaction used in ref. [46] explains the overall variation of charge radii by correcting the original interaction [49] for the agreement of 0_2^+ state by subtracting the double counting of pairing renormalization.

In shell model picture, in the ground state of ${}^{52}\text{Ca}$ the $f_{7/2}$ and $p_{3/2}$ orbitals are nearly fully occupied, causing a subshell gap at $N = 32$. This does not imply that the ${}^{52}\text{Ca}$ charge radius is the same as those of ${}^{40,48}\text{Ca}$ since the BE/A also affects the nuclear size, as evidenced by the data in Fig. 2. The large fragmentation of the wave functions, covering the active neutron $f_{5/2}, p_{3/2}, p_{1/2}$ orbitals separate from the first intruder $f_{7/2}$ orbital, is the possible reason behind the large value of the isotopic shift in ${}^{52}\text{Ca}$. This may be attributed to the location of the spin-orbit partners $f_{7/2}$ and $f_{5/2}$ [37]: a higher spin-orbit splitting leads to a larger charge radius. This mechanism is also known in ${}^{208}\text{Pb}$ region where the intruder orbital and its spin-orbit partner, $i_{13/2}$ and $i_{11/2}$, have many orbitals lying in between them [50]. Also, the N/Z ratio is

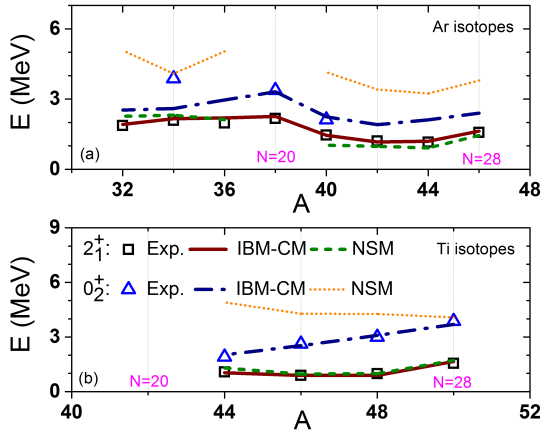


FIG. 6. (Color online) Experimental [24] and calculated energies E of the yrast 2_1^+ and yrare 0_2^+ levels in even-even (a) $^{32-46}\text{Ar}$ and (b) $^{44-50}\text{Ti}$ isotopes.

almost the same in ^{52}Ca and ^{212}Pb .

For comparison, we also show in Fig. 4 the isotopic shift taken from the Hartree-Fock nuclear mass table, as HFBCS-1 [51]. This approach reproduces the overall evolution of charge radii in the even-even $^{36-52}\text{Ca}$ isotopes, including the large value at ^{52}Ca , but not the dip in the isotopic shift at $N = 28$.

We use the same parameters η_{reg} and η_{int} to calculate the $\rho^2(E0; 0_2^+ \rightarrow 0_1^+)$ values in the even-even $^{40-48}\text{Ca}$ isotopes. The results are compared with the experimental data [25], where known, in Fig. 5. No calculated result is shown for ^{40}Ca , as it is taken as the inert core. In ^{42}Ca the calculated $\rho^2(E0; 0_2^+ \rightarrow 0_1^+)$ value deviates from the data, as was the case for its isotopic shift. In $^{44,48}\text{Ca}$, on the other hand, the IBM-CM results are in reasonable agreement with the data. This suggests the existence of a correlation between the charge radii of ground states and the energy of 0_2^+ levels, which in turn influences the $0_2^+ \rightarrow 0_1^+$ $E0$ transitions. The $\rho^2(E0; 0_2^+ \rightarrow 0_1^+)$ values are very small in both ^{40}Ca and ^{48}Ca , hinting at a possible connection between the location of 0_2^+ states and evolution of shell gaps.

B. The argon and titanium isotopes

We further perform IBM-CM calculations for the even-even $^{32-46}\text{Ar}$ and $^{44-50}\text{Ti}$ isotopes using the parameters as listed in Table I. ^{40}Ca is taken to be core. The excitation energies of the 2_1^+ and 0_2^+ levels calculated with the IBM-CM are compared with the experimental data in Fig. 6. In the Ar isotopes the IBM-CM results agree very well with the data except for ^{34}Ar where the predicted 0_2^+ is much lower in energy than observed as shown in Fig. 6(a). The measurement of 0_2^+ state in neighboring $^{32,36}\text{Ar}$ isotopes may help in future analysis. The spectroscopy in neutron-deficient $^{32-36}\text{Ar}$ isotopes is very lim-

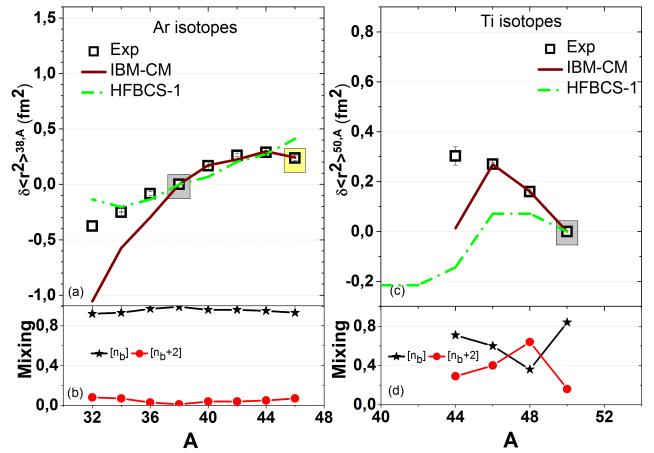


FIG. 7. (Color online) (a) Experimental [39–41] and calculated isotopic shifts in the even-even $^{32-46}\text{Ar}$ isotopes. Results of IBM-CM, and HFBCS-1 [51] calculations are shown. The stable semi-magic isotope is indicated in grey while the unstable semi-magic isotope is in yellow. (b) The mixing of the $[n_b]$ and $[n_b + 2]$ spaces for the ground states of the even-even $^{32-46}\text{Ar}$ isotopes. (c) and (d) are same as (a) and (b) but for the even-even $^{44-50}\text{Ti}$ isotopes.

ited, which hinders a satisfactory IBM analysis. In the Ti isotopes the agreement between the IBM-CM results and the data is quite nice for all the considered isotopes in Fig. 6(b). We also compare with NSM energies for both the Ar and Ti isotopes in Fig. 6. The NSM results in both chains explain the yrast 2_1^+ state while overestimating the energy of the yrare 0_2^+ level except in ^{34}Ar and ^{50}Ti .

With bosonic wave functions fixed from level energies, we compute the isotopic shifts in the even-even $^{40-46}\text{Ar}$ isotopes in Fig. 7(a), with fixed fitted values for $\kappa_{\text{reg}} = 0.024 \text{ fm}^2$, $\eta_{\text{reg}} = 5.47 \text{ fm}^2$, and $\eta_{\text{int}} = 0.01 \text{ fm}^2$. These parameters are then used to estimate the isotopic shifts in the even-even $^{32-38}\text{Ar}$ isotopes, which were further normalized with respect to ^{38}Ar to compare with data. The mixing of the $[n_b]$ and $[n_b + 2]$ spaces in the IBM-CM is shown in Fig. 7(b) for the ground states of the even-even $^{32-46}\text{Ar}$ isotopes. A very weak mixing appears to be reasonable in all the considered Ar isotopes with a relatively pure configuration in the semi-magic stable nucleus ^{38}Ar . The 0_2^+ state in ^{38}Ar mainly arises due to the core-excitations as was expected in the $E0$ measurement conducted in 1975 [52], though IBM-CM analysis could not explain the corresponding order of $\rho^2(E0)$. The very large value of χ parameter required to reproduce the level energies in $^{32,34,36}\text{Ar}$ eventually influences the \hat{n}_d matrix elements in both the regular and intruder IBM configuration spaces, leading to a larger deformation effects controlling the charge radii if compared to neighboring Ca isotopes.

A similar IBM-CM study is made for the even-even $^{44-50}\text{Ti}$ isotopes, the results of which are shown in

Fig. 7(c) with $\kappa_{\text{reg}} = -0.0002 \text{ fm}^2$, $\eta_{\text{reg}} = 4.1 \text{ fm}^2$, and $\eta_{\text{int}} = -1.5 \text{ fm}^2$. The calculation could not explain the charge radius of ^{44}Ti . The mixing of $[n_b]$ and $[n_b + 2]$ spaces in the ground states of these Ti isotopes is depicted in Fig. 7(d). A relatively pure $[n_b]$ space is found in semi-magic ^{50}Ti with χ parameter being nearly zero. In $^{44,46,48}\text{Ti}$ isotopes, a large value of χ parameter for explaining the level energies, eventually influences the deformation effects arising from \hat{n}_d matrix elements in IBM-CM analysis and consequently, changing the charge radii. The Table III lists the mixing probabilities obtained in the IBM-CM analysis for the first 2_1^+ and excited 0_2^+ states in these Ti isotopes. It may be noted that the mixing supported by the first 2_1^+ state for $^{46,48}\text{Ti}$ in their bosonic wave functions is in line with the measured g -factor values [53], suggesting them to be of collective character.

The NSM results on the charge radii for both the Ar and Ti isotopic chains are not known in literature, and could not be estimated in absence of the interaction by Caurier *et al.* [46]. The semi-magic ^{38}Ar is clearly more stable to the next semi-magic ^{46}Ar , as also shown in Fig. 7(a). The difference in BE/ A explains qualitatively why the charge radii in the two semi-magic Ar isotopes, ^{38}Ar and ^{46}Ar , are quite different, in contrast to the $^{40,48}\text{Ca}$ isotopes, which have similar BE/ A and equal charge radii. The same can be expected for ^{42}Ti due to the difference in BE/ A to behave differently than the other semi-magic stable ^{50}Ti isotope. The future measurement of spectroscopy as well as charge radii in ^{42}Ti would be interesting in this regard. This is simply because binding of nucleons reflected in binding energy can govern the overall nuclear size and the charge radii. More tightly bound the nucleons are, lesser is the charge radius. Similarity in the charge radii of $^{40,48}\text{Ca}$ isotopes is not only due to the doubly-magic configurations involved but also due to their similar binding energies which is not the case for the Ar and Ti isotopic chains.

IV. CONCLUSIONS

The nuclear size, that is, isotopic shift for charge radii of the even-even $^{36-52}\text{Ca}$, $^{32-48}\text{Ar}$, and $^{44-50}\text{Ti}$ has been

studied in terms of the IBM-CM. A near-spherical nature of $^{36-52}\text{Ca}$ isotopes is obtained, although core excitations are necessary to describe the yrare states. Bosonic wave functions are first fixed using the agreement of level energies and then used to compute the isotopic shift of charge radii in $^{36-52}\text{Ca}$ isotopes. The $E0$ transitions connecting 0_2^+ states to 0_1^+ states are correlated with the isotopic shift of charge radii in Ca isotopes where $\rho^2(E0; 0_2^+ \rightarrow 0_1^+)$ data are also available for the comparison. With the obtained bosonic wave functions, a study on even-even Ar and Ti isotopes is also presented for the isotopic shift of charge radii. The BE/ A qualitatively explains the similarity of charge radius in ^{40}Ca and ^{48}Ca , and difference of charge radius in ^{38}Ar and ^{46}Ar , and ^{42}Ti and ^{50}Ti . It may be mentioned that the powerful connection between nuclei and neutron stars, encoded in the nuclear equation of state, in which the nuclear symmetry energy (i.e., the cost of converting symmetric nuclear matter into pure neutron matter) is used to set the basis of long-planned radius experiments at JLab [54, 55]. The current analysis provides an additional perspective for the same.

ACKNOWLEDGMENTS

The author BM gratefully acknowledges the financial support from the HORIZON-MSCA-2023-PF-01 project, ISOON, under grant number 101150471. The funding from the Croatian Science Foundation and the École Polytechnique Fédérale de Lausanne, under the project TTP-2018-07-3554 “Exotic Nuclear Structure and Dynamics”, with funds of the Croatian-Swiss Research Programme is also acknowledged for enabling the initiation of this work.

-
- [1] M. Goeppert-Mayer and J. H. D. Jensen, *Elementary theory of nuclear shell structure* (Wiley, New York, 1955).
 - [2] T. Otsuka, A. Gade, O. Sorlin, T. Suzuki, and Y. Utsuno, *Rev. Mod. Phys.* **92**, 015002 (2020).
 - [3] A. Ozawa, T. Kobayashi, T. Suzuki, K. Yoshida, and I. Tanihata, *Phys. Rev. Lett.* **84**, 5493 (2000).
 - [4] T. Otsuka, R. Fujimoto, Y. Utsuno, B. A. Brown, M. Honma, and T. Mizusaki, *Phys. Rev. Lett.* **87**, 082502 (2001).
 - [5] O. Sorlin and M.-G. Porquet, *Prog. in Part. Nucl. Phys.* **61**, 602 (2008).
 - [6] T. Otsuka, T. Suzuki, R. Fujimoto, H. Grawe, and Y. Akaishi, *Phys. Rev. Lett.* **95**, 232502 (2005).
 - [7] A. J. Miller *et al.*, *Nature Phys.* **15**, 432 (2019).
 - [8] R. F. Garcia Ruiz *et al.*, *Nat. Phys.* **12**, 594 (2016).
 - [9] F. Iachello and A. Arima, *The interacting boson model* (Cambridge University Press, 1987).
 - [10] S. Zerguine, P. Van Isacker, A. Bouldjedri, and S. Heinze, *Phys. Rev. Lett.* **101**, 022502 (2008).
 - [11] S. Zerguine, P. Van Isacker, and A. Bouldjedri, *Phys. Rev. C* **85**, 034331 (2012).
 - [12] P. Van Isacker, *Nucl. Data Sheets* **120**, 119 (2014).

- [13] K. Nomura, R. Rodríguez-Guzmán, and L. M. Robledo, *Phys. Rev. C* **87**, 064313 (2013).
- [14] C. Force *et al.*, *Phys. Rev. Lett.* **105**, 102501 (2010).
- [15] T. Mizusaki, T. Otsuka, M. Honma, and B. A. Brown, *Phys. Rev. C* **63**, 044306 (2001).
- [16] J.-P. Delaroche, M. Girod, J. Libert, H. Goutte, S. Hilaire, S. Péru, N. Pillet, and G. F. Bertsch, *Phys. Rev. C* **81**, 014303 (2010).
- [17] https://www-phynu.cea.fr/science_en_ligne/carte_potentiels_microscopiques/carte_potentiel_nucleaire_eng.htm
- [18] K. Heyde and J.L. Wood, *Rev. Mod. Phys.* **83**, 1467 (2011).
- [19] B. Maheshwari and K. Nomura, *J. Phys. G: Nucl. Part. Phys.* **51**, 095101 (2024).
- [20] P. Garrett, M. Zielinska, and E. Clement, *Prog. Part. and Nucl. Phys.* **124**, 103931 (2022).
- [21] S. Leoni, B. Fornal, A. Bracco, Y. Tsunoda, and T. Otsuka, *Prog. Part. and Nucl. Phys.* **139**, 104119 (2024).
- [22] S. Gorodetzky, N. Schulz, J. Chevallier, and A. C. Knipper, *J. Phys. (Paris)* **27**, 521 (1966).
- [23] N. Schulz, *Ann. Phys. (Paris)* **2**, 81 (1967).
- [24] Evaluated Nuclear Structure Data File, <https://www.nndc.bnl.gov/ensdf/>.
- [25] T. Kibedi, A. B. Garnsworthy, and J. L. Wood, *Prog. Part. Nucl. Phys.* **123**, 103930 (2022).
- [26] P. D. Duval and B. R. Barrett, *Phys. Lett. B* **100**, 223 (1981).
- [27] A. Arima and F. Iachello, *Phys. Rev. Lett.* **35**, 1069 (1975).
- [28] T. Otsuka, A. Arima, and F. Iachello, *Nucl. Phys. A* **309**, 1 (1978).
- [29] P. Van Isacker, IBM-1 code, unpublished.
- [30] J.P. Elliott and A.P. White, *Phys. Lett. B* **97**, 169 (1980).
- [31] J.P. Elliott and J.A. Evans, *Phys. Lett. B* **101**, 216 (1981).
- [32] V.S. Lac, J.P. Elliott, J.A. Evans and G.L. Long, *Nucl. Phys. A* **587**, 101 (1995).
- [33] M. K. Harder, K. T. Tang, and P. Van Isacker, *Phys. Lett. B* **405**, 25 (1997).
- [34] I. Angeli, and K. P. Marinova, *Atomic Data and Nuclear Data Tables* **99**, 69 (2013).
- [35] N. Shimizu, T. Mizusaki, Y. Utsuno, and Y. Tsunoda, *Comp. Phys. Comm.* **244**, 372 (2019).
- [36] Y. Utsuno, T. Otsuka, B. A. Brown, M. Honma, T. Mizusaki, and N. Shimizu, *Phys. Rev. C* **86**, 051301 (R) (2012).
- [37] A. Poves, J. Sanchez-Solano, E. Caurier, and F. Nowacki, *Nucl. Phys. A* **694**, 157 (2001).
- [38] K.-H. Speidel *et al.*, *Phys. Rev. C* **78**, 017304 (2008).
- [39] K. Blaum, W. Geithner, J. Lassen, P. Lievens, K. Marinova, and R. Neugart, *Nucl. Phys. A* **799**, 30 (2008).
- [40] H. D. Wohlfahrt, E. B. Shera, M. V. Hoehn, Y. Yamazaki, and R. M. Steffen, *Phys. Rev. C* **23**, 533 (1981).
- [41] A. Anastassov, Yu. P. Gangrsky, K. P. Marinova, B. N. Markov, and S. G. Zemlyanoi, *Z. Phys. D* **30**, 275 (1994).
- [42] National Nuclear Data Center, <https://www.nndc.bnl.gov/>.
- [43] https://www.chem.ualberta.ca/~massspec/atomic_mass_abund.pdf
- [44] A. R. L. Kennington *et al.*, *Phys. Rev. C* **103(3)**, 035805 (2021).
- [45] L. Lalanne *et al.*, *Phys. Rev. Lett.* **129**, 122501 (2022).
- [46] E. Caurier, K. Langanke, G. Martínez-Pinedo, F. Nowacki, and P. Vogel, *Phys. Lett. B* **522**, 240 (2001).
- [47] T. Otsuka, Y. Tsunoda, T. Abe, N. Shimizu, and P. Van Duppen, *Phys. Rev. Lett.* **123**, 222502 (2019).
- [48] R. A. Ricci and P. R. Maurenzig, *Riv. Nuovo Cimento* **1**, 291 (1969).
- [49] J. Retamosa, E. Caurier, F. Nowacki, and A. Poves, *Phys. Rev. C* **55**, 1266 (1997).
- [50] M. Bhuyan *et al.*, *J. Phys. G: Nucl. Part. Phys.* **48**, 075105 (2021).
- [51] S. Goriely, F. Tondeur, and J. M. Pearson, *Atomic Data and Nuclear Data Tables* **77**, 311 (2001).
- [52] K. H. Souw, J. C. Adloff, D. Disdier, and P. Chevallier, *Phys. Rev. C* **12**, 1103 (1975).
- [53] R. Ernst *et al.*, *Phys. Rev. Lett.* **84**, 416 (2000).
- [54] D. Adhikari *et al.* (CREX), *Phys. Rev. Lett.* **129**, 042501 (2022).
- [55] D. Adhikari *et al.* (PREX), *Phys. Rev. Lett.* **126**, 172502 (2021).